Chinese Chemical Letters 34 (2023) 108518

Contents lists available at ScienceDirect

Chinese Chemical Letters

journal homepage: www.elsevier.com/locate/cclet

Self-oxygenated co-assembled biomimetic nanoplatform for enhanced photodynamic therapy in hypoxic tumor

Bingchen Zhang[a,b,1], Ling Lin[a,1], Jizong Mao[c], Weisheng Mo[c], Zibo Li[a], Shengtao Wang[d], Yan Tang[a], Chunhui Cui[c,*], Yifen Wu[b,*], Zhiqiang Yu[a,*]

[a] Department of Laboratory Medicine, Dongguan Institute of Clinical Cancer Research, Affiliated Dongguan Hospital, Southern Medical University, Dongguan 523058, China
[b] Dongguan Institute of Clinical Cancer Research, Dongguan Key Laboratory of Precision Diagnosis and Treatment for Tumors, Affiliated Dongguan Hospital, Southern Medical University, Dongguan 523058, China
[c] Department of General Surgery, Zhujiang Hospital, Southern Medical University, Guangzhou 510280, China
[d] Affiliated Foshan Maternity & Child Healthcare Hospital, Southern Medical University (Foshan Maternity & Child Healthcare Hospital), Foshan 528000, China

ARTICLE INFO

Article history:
Received 9 February 2023
Revised 23 April 2023
Accepted 26 April 2023
Available online 4 May 2023

Keywords:
Photodynamic therapy
Biomimetic nanoplatform
Self-oxygenated co-assembly nanoparticles
Immunogenic cell death
HIF-1α-CD39-CD73-A2AR pathway

ABSTRACT

Photodynamic therapy (PDT) has shown great application potential in cancer treatment and the important manifestation of PDT in the inhibition of tumors is the activation of immunogenic cell death (ICD) effects. However, the strategy is limited in the innate hypoxic tumor microenvironment. There are two key elements for the realization of enhanced PDT: specific cellular uptake and release of the photosensitizer in the tumor, and a sufficient amount of oxygen to ensure photodynamic efficiency. Herein, self-oxygenated biomimetic nanoparticles (CS@M NPs) co-assembled by photosensitizer prodrug (Ce6-S-S-LA) and squalene (SQ) were engineered. In the treatment of triple negative breast cancer (TNBC), the oxygen carried by SQ can be converted to reactive oxygen species (ROS). Meanwhile, glutathione (GSH) consumption during transformation from Ce6-S-S-LA to chlorin e6 (Ce6) avoided the depletion of ROS. The co-assembled (CS NPs) were encapsulated by homologous tumor cell membrane to improve the tumor targeting. The results showed that the ICD effect of CS@M NPs was confirmed by the significant release of calreticulin (CRT) and high mobility group protein B1 (HMGB1), and it significantly activated the immune system by inhibiting the hypoxia inducible factor-1alpha (HIF-1α)-CD39-CD73-adenosine a2a receptor (A2AR) pathway, which not only promoted the maturation of dendritic cells (DC) and the presentation of tumor specific antigens, but also induced effective immune infiltration of tumors. Overall, the integrated nanoplatform implements the concept of multiple advantages of tumor targeting, reactive drug release, and synergistic photodynamic therapy-immunotherapy, which can achieve nearly 90% tumor suppression rate in orthotopic TNBC models.

Triple negative breast cancer (TNBC) is the most aggressive subtype of breast cancer with no efficient treatment and high mortality [1,2]. As the breast cancer has become the most common global malignancy and the leading cause of cancer death, the research on the new treatment strategy for TNBC is badly urgent [3]. Photodynamic therapy (PDT) has been approved as a formal clinical treatment strategy in several countries [4]. By laser excitation with a specific wavelength, the photosensitizer transfers energy to the surrounding oxygen, generating highly active singlet oxygen that leading to cytotoxic effect [5–9]. Although TNBC is a superficial tumor that conducive to laser penetration, the tumor hypoxic environment severely limits the efficacy of PDT [10,11]. In addition to the lack of adequate oxygen supply for photosensitizer, the overexpression of hypoxia-inducible factor-1alpha (HIF-1α) in tumor environment activates the CD39-CD72-adenosine a2a receptor (A2AR) pathway, which inhibits the immune response of immune cells [9]. Therefore, it is an effective way to enhance the efficiency of photodynamic therapy by overcoming the tumor hypoxic environment. Squalene (SQ) is a natural product of homology of medicine and food with good biosafety [12]. In addition to the anti-cancer properties as reported, SQ has a function similar to oxygen uptake by red blood cells and efficiently combine with oxygen to produce activated oxidized squalene, which realizes the oxygen release in

* Corresponding authors.
E-mail addresses: drcuich@163.com (C. Cui), 35662369@qq.com (Y. Wu), yuzq@smu.edu.cn (Z. Yu).
[1] These authors contributed equally to this work.

https://doi.org/10.1016/j.cclet.2023.108518
1001-8417/

cells [13]. However, SQ has the same application barriers as photosensitizers such as porphyrin or chlorin, with poor water solubility and poor targeting [14,15]. Therefore, the key to enhancing PDT for the treatment of TNBC is to figure out how to build a novel self-oxygenating nano-delivery platform based on SQ.

In recent years, the research on the drug delivery system has become the focus of field [16,17], and the development of nanotechnology exhibited the promising potential for the drug delivery in the cancer treatment [18–20]. As the novel nanodelivery system, the concept of "self-assembled nanoprodrug" has received increasing attention [21–23]. The combined benefits of innovative prodrug strategies and carrier-free delivery systems make such nanoplatforms more efficient in cancer therapy [24,25]. Linoleic acid (LA) is an essential fatty acid for the fatty acid metabolism in human body that has been reported to achieve the self-assembly properties of micro-molecule [26]. For instant, Wang *et al.* reported a series of novel self-assembly nanosysem based on LA for hydrophobic drugs delivery *in vivo* [27,28]. Meanwhile, the self-assembly nanoparticles based on the chlorin e6 (Ce6) was also reported, it exhibited the excellent drug delivery and cancer treatment [29]. The system is characterized by simple preparation, high repeatability, slow degradation and long half-life. In addition, the introduction of disulfide bond is able to ensure specific release of drugs from self-assembly nanodrug in high glutathione (GSH) environment of tumors, resulting in the structural destruction of prodrug [30,31]. The preparation strategy of precursor drugs efficiently improves the adverse physical and chemical properties of drugs, enhancing the stability and solubility of drugs, and avoiding the occurrence of non-selective toxicity [32–35]. After the construction of self-assembled prodrug, the preparation of bionic system by tumor cell membrane becomes a better choice with many advantages [36,37]. By homologous targeting, nanosystems have efficient tumor aggregation and lower immunogenicity to avoid being engulfed by the immune system [38].

Herein, we reported a homologous tumor cell membrane camouflaged self-assembly nanoplatform with oxygen supply function for TNBC combination photodynamic-immunotherapy. Ce6 was synthesized with LA by disulfide bond, and we found that it can effectively bind SQ and formed an integrated self-assembled nanoprodrug (CS NPs). After that, the biomimetic self-assembled nanodrug (CS@M NPs) was obtained by wrapping TNBC cell membrane (Scheme 1A). The preparation process was extremely simple due to the cell membrane directly clad on the surface of the self-assembled nanodrug. There was no requirement to resort to the structural frameworks such as poly(lactic-*co*-glycolic acid) (PLGA) or other adjuvants. As shown in Scheme 1B, biomimetic achieved specific self-recognition of tumors after intravenous injection, and cell membranes fuse and break to release self-assembled nanoprodrug. Disulfide bonds consumed GSH and the stimulation of GSH gave rise to the immolation of itself, resulting in the Ce6 and oxygen-carried SQ entered into the tumor cells. SQ had the cytotoxicity for tumor cells, as well as supplied oxygen to Ce6 to generate the reactive oxygen species (ROS) for efficient PDT with redox-imbalance. Moreover, the reversal of hypoxic environment inhibited the expression of HIF-1α, thereby relieving the inhibition of A2AR on dendritic cells (DC) and T cells. At the same time, immunotherapy effect was greatly enhanced by combining with the immunogenic cell death (ICD) effect of PDT on tumor cells. It indicated that the strategy was allowed to the efficient delivery of muti-drugs and engendered broad opportunities for practical use.

The prodrug of Ce6 (Ce6-S-S-LA) was synthesized as shown in Fig. S1 (Supporting information) and characterized by nuclear magnetic resonance hydrogen spectrum (^{1}H NMR) and electro spray ionization-mass spectroscopy (ESI-MS) (Figs. S2 and S3 in Supporting information). CS NPs was obtained through the self-assembly of Ce6-S-S-LA and SQ by the solvent exchange methods. The optimization of the preparation process of CS NPs and the characterization under the most available process are shown in Table S1 and Table S2 (Supporting information), respectively. Afterwards, the 4T1 cell membrane was used to wrap the CS NPs to prepare CS@M NPs. As shown in Fig. 1A, the average diameters for CS NPs and CS@M NPs were 96.3 nm and 118 nm, and the corresponding zeta potentials were −14.8 mV and −18.6 mV, respectively. By testing the integrality of cell membrane proteins, the successful cell membrane binding of CS@M NPs was confirmed by the Coomassie brilliant blue and agarose gels compared to the cells (Fig. 1B). The similar particle sizes and the good dispersity of CS NPs and CS@M NPs were observed by atomic force microscope (AFM) (Fig. 1C). The results of TEM revealed that, in comparison to CS NPs, CS@M NPs had an additional 4T1 cell membrane shell that was about 15–20 nm thick (Fig. 1D). Ce6 and SQ were quantified based on the ultraviolet–visible (UV–vis) and fluorescence spectra (Figs. 1E and F). Based on the disulfide bond in the Ce6-S-S-LA structure and the GSH response, solutions containing different concentrations of GSH were used to determine the *in vitro* release characteristics of the nanoparticles. As shown in Fig. 1G, the average cumulative release of Ce6 and SQ was correlated with the GSH concentration and was positively correlated. When the GSH concentration was 10 mmol/L, the release amounts of Ce6 and SQ exceeded 80% and 70%, respectively. This result indicated that the nanoparticle structure collapses and was accompanied by the breakage of disulfide bonds in the tumor's high GSH environment, which results in the effective release of drugs. The stability of nanoparticles in long-term storage and different physiological environments were investigated, respectively. Fig. S4 (Supporting information) showed that the particle sizes of CS NPs and CS@M NPs did not change significantly after 14 days. The high stability of nanoparticles was further demonstrated in various internal physiological environments simulated by 0.9% NaCl solution, Dulbecco's modified eagle medium (DMEM), and DMEM+5% fetal bovine serum (FBS) (Fig. S5 in Sup-

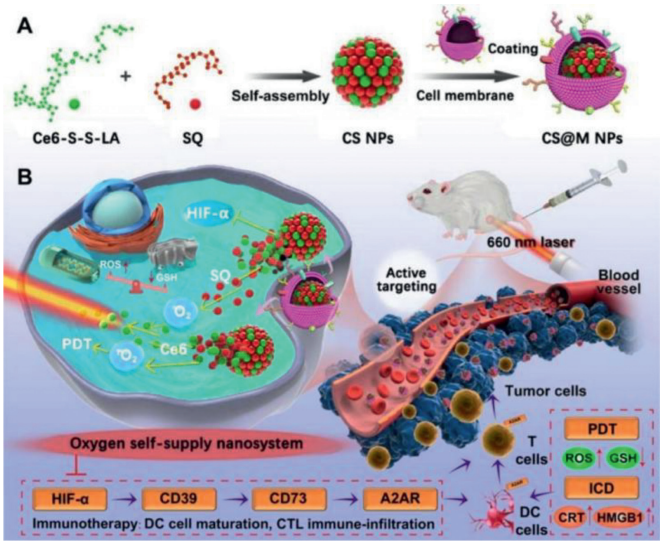

Scheme 1. Schematic illustration of self-oxygenated biomimetic nanodrug (CS@M NPs) based on enhanced PDT strategy for TNBC treatment. (A) Synthesis of CS@M NPs. (B) Multi-mechanism of CS@M NPs in enhanced PDT-based treatment of hypoxic tumors: (1) Bionic cell membrane enabled nanoparticles to target tumors and achieve high accumulation. (2) SQ and Ce6 were released in response to high levels of GSH in tumor cells, and the oxygen carried by SQ enhanced the photodynamic efficiency of Ce6 under 660 nm radiation. The imbalance between sharply increased ROS and consumed GSH led to significant death of tumor cells. (3) Meanwhile, with the reversal of hypoxic microenvironment in tumor cells, immune system was activated by inhibiting the HIF-1α-CD39-CD73-A2AR pathway. The ICD effect further promoted the presentation of tumor-specific antigens for mature DC and the efficient tumor immune infiltration by cytotoxicity T cells.

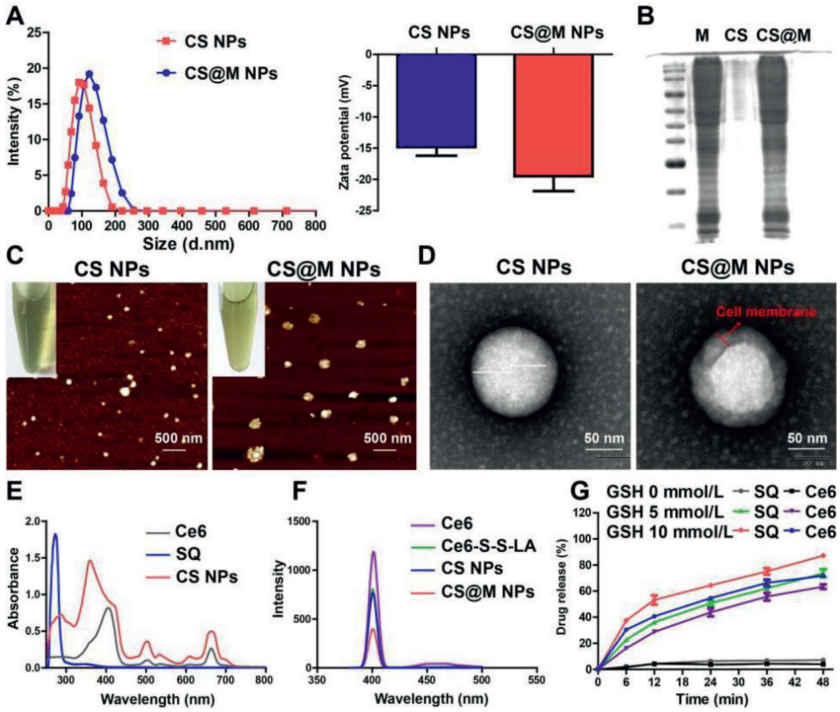

Fig. 1. Characterization of CS NPs and CS@M NPs. (A) The particle sizes and zeta potentials of CS NPs and CS@M NPs. (B) Cell membrane proteins on the surface of CS@M NPs were verified by Coomassie brilliant blue staining and polyacrylamide gel electrophoresis. (C, D) AFM images (Scale bar: 500 nm) and TEM images (Scale bar: 50 nm) of CS NPs and CS@M NPs. (E) UV–vis spectrum of Ce6, SQ and CS NPs. (F) Fluorescence spectrum of Ce6, Ce6-S-S-LA, CS NPs and CS@M NPs. (G) *In vitro* release of triggered by different concentrations of GSH.

porting information). Molecular mimicry performed in DS4.5 revealed that the possible co-assembly principle of CS NPs based on the LA and Ce6 was hydrophobic interactions, including hydrogen bonding and π-π stacking (Fig. S6 in Supporting information). In Fig. S7 (Supporting information), the particle size of CS NPs varied significantly in a 5% sodium dodecyl sulfate (SDS) solution, since SDS achieved the disruption of the structure of CS NPs by affecting the hydrophobic interactions.

The relative GSH ratios of 4T1 cells treated with different drugs were measured by a GSH assay kit. As shown in Fig. S8A (Supporting information), compared with the other groups, the nanoparticle groups effectively reduced the endogenous GSH content and disrupted the original redox balance. The dissolved oxygen content in solution was measured over a continuous period of 12 min to assess the self-oxygenated efficiency of CS NPs and CS@M NPs. The results revealed that SQ had a notable oxygenation efficiency, and the nanoparticles further prolonged the oxygen supply while maintaining its volume (Fig. S8B in Supporting information). In addition, the fluorescence absorption of the 9,10-anthracenediyl-bis(methylene)dimalonic acid (ABDA) probe showed that the CS NPs and CS@M NPs groups had higher ROS production efficiency than other free photosensitizers in 4T1 cells (Fig. S8C in Supporting information). HIF-1α antibody was used to investigate the reversal of the hypoxic microenvironment of 4T1 cells by self-oxygenating nanoparticles in the presence of PDT. Fig. S8D (Supporting information) showed that free SQ relieved cellular hypoxia to some extent, and the CS@M NPs had the best effect on remodeling redox equilibrium. The above results showed that SQ provided sufficient oxygen for enhancing the efficiency of PDT, which generated large amounts of ROS and consumed GSH and improved cellular hypoxia by reshaping the intracellular redox balance.

In 4T1 cells and HeLa cells, studies on the cellular uptake of nanoparticles were conducted. Co-assembly with the amphiphilic dye indocyanine green angiography (ICG) was used to fluorescently label CS NPs and CS@M NPs. The semi-quantitative flow cytometry (FCM) results and intracellular fluorescence distribution determined by laser scanning confocal microscopy (CLSM) indicated that 4T1 cells were the most effective in CS@M NPs uptake (Fig. 2A). In contrast, HeLa cells did not show any discernible differences in the uptake of CS NPs and CS@M NPs (Fig. S9 in Supporting information). The tumor enhanced permeability and retention effect (EPR) effect and homologous targeting of tumor cell membranes enabled the CS@M NPs to successfully increase the nanoparticle delivery efficiency. 2′,7′-Dichlorodihydrofluorescein diacetate (DCFH-DA) probe was used to test the intracellular ROS generation in 4T1 cells. The results showed that the weakest green fluorescence of DCF was present in the SQ group after 4 h of incubation with different formulations of drugs, and the intensity of green fluorescence was similar in the CS NPs, CS@M NPs and Ce6 groups. In addition, the nanoparticles continued to exhibit significant ROS activation effects over time compared to the free drug groups (Fig. S10 in Supporting information). At 12 h of drug treatment and exposure to laser, the CS@M NPs group exhibited the highest efficiency of intracellular ROS generation, reflecting the increased efficiency of PDT (Fig. 2B).

The inhibition of the activity of each formulation on 4T1 cells and MDA-MB-231 cells was determined by cell counting kit-8 (CCK8). The molar concentration ratio of Ce6 and SQ in CS NPs and CS@M NPs was known to be close to 1:1. The specific group settings were as follows: normoxic/dark, normoxic/laser, hypoxic/dark, and hypoxic/laser. The results showed the concentration-dependent toxicity of Ce6 and SQ on 4T1 cells under hypoxic and normoxic conditions. Notably, cells exposed to normoxia and hypoxia were similarly inhibited by the nanoparticles in the absence of lasers. Contrarily, when exposed to laser light, the cytotoxic differentiation of nanoparticles under normoxic conditions was less pronounced than it was under hypoxic conditions. And the cytotoxicity of nanoparticles under laser conditions were greater compared to the dark conditions. The aforementioned findings indicated that PDT had a cytocidal effect,

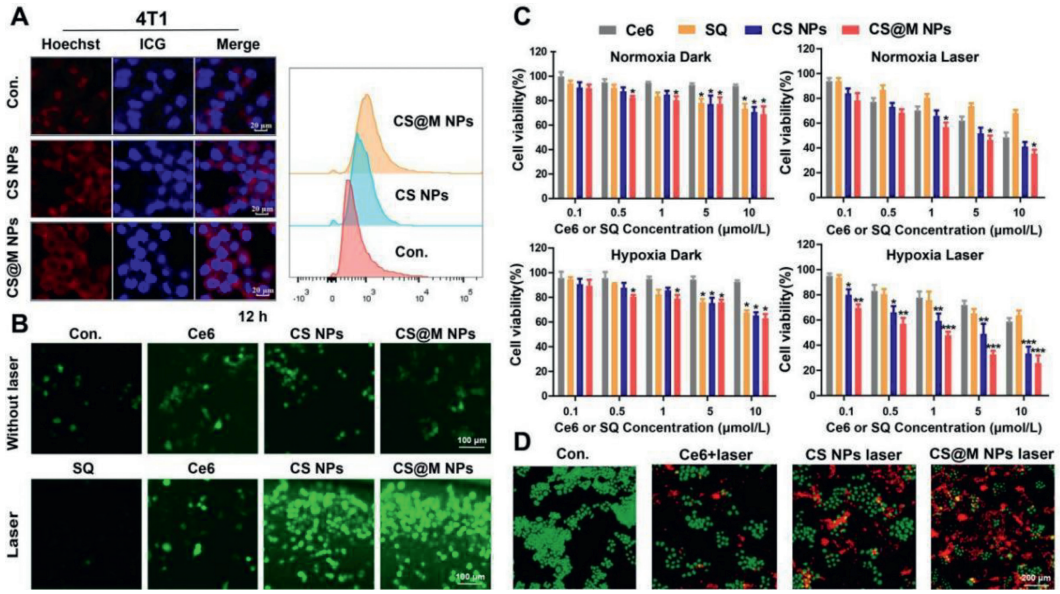

Fig. 2. Cellular uptake and cytotoxicity of CS@M NPs in TNBC cells. (A) Cellular uptake of 4T1 cells measured by CLSM and FCM. Scale bar: 50 μm. (B) Intracellular ROS levels in 4T1 cells measured by DCFH-DA staining. Scale bar: 100 μm. (C) Relative cell viabilities of 4T1 cells at 48 h post treatment. (D) Fluorescence microscopic images of 4T1 cells with calcein-AM/PI staining. Scale bar: 200 μm. The results were expressed as the mean ± standard deviation (SD) ($n = 3$). $^{*}P < 0.05$, $^{**}P < 0.01$, $^{***}P < 0.001$ represent a significant difference between groups.

and self-oxygenated nanoparticles were successful in boosting PDT and enhancing cytostatic effects in hypoxic cells (Fig. 2C). As proved in Fig. S11 (Supporting information), the level of oxygen radical in tumor cells under hypoxia was lower than that cells in normoxic environment, and the expression level of GSH for REDOX equilibrium was also lower. It leaded to the tumor cells in hypoxic environment were more sensitive to the large amounts of ROS produced by photodynamic therapy. Similar outcomes were attained in MDA-MB-231 cells treated with SQ, Ce6, CS, and CS@M NPs, as shown in Fig. S12 (Supporting information). There are two possible reasons for that the cytotoxicity of CS@M NPs in the hypoxia/laser group better than CS NPs. On the one hand, CS@M NPs entered into tumor cells through membrane fusion, which has stronger delivery efficiency than CS NPs. On the other hand, the encapsulation of the cell membrane provided better protection for the internal oxygen-binding of nanodrug, so as to avoid the destruction and oxygen loss of CS caused by the stimulation of excreted GSH of tumor cells before entering the cells. The calculation of the combination index (CI) quantified the degree of synergism between Ce6 and SQ in CS NPs, and CI < 1 indicated the presence of synergistic effects (Fig. S13 in Supporting information). The apoptotic effects of the different formulations were further explored by calcein-AM/propidium iodide (PI) double staining assays in 4T1 cells, which showed that CS@M NPs+Laser had the most significant cytotoxicity (Fig. 2D). And CS@M NPs achieved effective cell death in both normoxic and hypoxic environments.

To further demonstrate the tumor targeting capacity of biomimetic CS@M NPs with homologous cell membrane encapsulation *in vivo*, the ICG was conjugated with the nanoparticles, and the fluorescence imaging of nanoparticles in an orthotopic breast tumor model was evaluated. The bioimaging results at different time points showed good accumulation of nanoparticles at the tumor site. The tumor site exhibited the greatest relative fluorescence intensity at 24 h. NIR-I imaging of excised organs also showed the highest concentration of nanoparticles in the tumor tissue at this time (Fig. S14 in Supporting information). In addition, both groups CS NPs and CS@M NPs showed better long circulation effects, tumor tissue targeting and high accumulation compared to the free ICG group. Compared with the accumulation of CS NPs due to the EPR effect, the CS@M NPs showed a further enhancement of the tumor targeting ability owing to the modification with the homologous cell membrane. The distribution of fluorescence in the tumor and major organs confirmed that the CS NPs had significantly enhanced tumor accumulation.

In vivo treatment was based on the same orthotopic TNBC tumor model, which was established by the inoculation of 4T1 cells. All animals used in these investigations were handled in accordance with protocol procedures, approved by the Institutional Animal Care and Use Committee of Southern Medical University. The mice were randomly divided into the following eight groups: (1) PBS, (2) SQ, (3) Ce6, (4) Ce6+Laser, (5) CS NP, (6) CS NPs+Laser (7) CS@M NPs, and (8) CS@M NPs+Laser. The tumor volume and weight of the phosphate belanced solution (PBS) group continued to increase during the 21-day experimental cycle, the CS@M NPs+Laser group showed the best treatment effect, and the remaining groups exhibited different degrees of tumor suppression (Figs. 3A–C and Fig. S15 in Supporting information). No significant weight loss was observed in the mice of the NPs group relative to the PBS group, which further confirmed the safety of the nanoparticles. Hematoxylin-eosin (HE) staining and terminal deoxynucleotidyltransferase-mediated dUTP nick-end labeling (TUNEL) staining of tumor tissues indicated that CS@M NPs led to significant tissue damage and cell death (Figs. 3D and E). The presence of HIF-1α in significant amounts in the tumor tissues of the PBS group confirmed the tumor's hypoxic condition, and PDT alone made the situation worse for the cells (Fig. 3F). In contrast, nanoparticles containing SQ significantly decreased HIF-1α expression and reversed tumor cell hypoxia through the self-oxygenation effect.

Through serum biochemical analysis, the impact of nanoparticles on the physiological environment of mice was examined (Fig. S16 in Supporting information). The results showed that the values of alanine aminotransferase (ALT), aspartate aminotransferase (AST), urea nitrogen (BUN), and creatinine (CRE) in the PBS group were significantly increased, suggesting that the carcinoma caused pathological reactions in the liver and kidney. The abovementioned indexes, however, demonstrated a decreasing trend in the CS@M NPs treatment group, indicating that CS@M NPs could

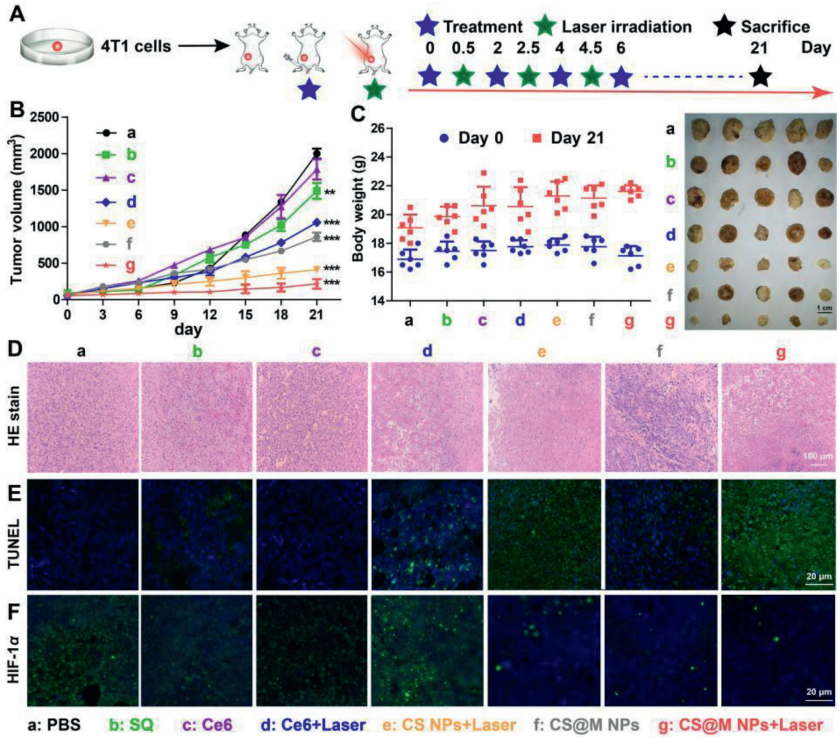

Fig. 3. Biodistribution and *in vivo* treatment of CS@M NPs. (A) Schematic illustration of therapeutic process with drugs intravenous injection and 660 nm laser irradiation. Tumor growth curves (B) and body weight (C) of 4T1 tumor-bearing mice post the indicated treatments in 21 days ($n = 5$). (D-F) HE, TUNEL and HIF-1α staining of tumors following the indicated treatments. Scale bar: 20 μm. The results were expressed as the mean ± SD ($n = 3$). $^{**}P < 0.01$, $^{***}P < 0.001$.

successfully promote the recovery of the physiological environment *in vivo*. Additionally, HE staining was used to assess the histological integrity of the heart, liver, spleen, lung, and kidney (Fig. S17 in Supporting information). And no significant damage was observed in the organs of mice in the nanoparticle treatment group. In conclusion, CS@M NPs have good biosafety and no significant side effects on normal tissues.

Through whole genome RNA sequencing of tumors, the potential biological mechanism of enhanced PDT-based treatment of TNBC by CS@M NPs was initially investigated. Exonic region detection results revealed that, compared to the PBS group, the CS@M NPs group had transcript upregulation in 721 genes and transcript downregulation in 105 genes out of 55,359 genes (Figs. S18A and B in Supporting information). CS@M NPs+Laser significantly affected multiple signaling pathways such as energy metabolism, inflammatory response, immune response, and apoptosis. The above pathways have been shown to be associated with adequate oxygen supply and PDT effects. In the differential gene cluster heat map, mechanistic target of rapamycin kinase (m-TOR), protein kinase AMP-activated catalytic subunit alpha (AMPK), and matrix metallopeptidase-9 (MMP-9) transcripts were upregulated due to increased energy metabolism brought on by oxygen supply from CS@M NPs, whereas CS@M NPs successfully induced apoptosis and immune activation, leading to upregulation of interleukin-2 (IL-2), C-X-C motif chemokine ligand 12 (CXCL12), interleukin-12 (IL-12), and caspase 3 (CASP3) expression (Fig. S18C in Supporting information). The graph of protein–protein interaction network showed ICD related genes of CS@M NPs group such as calreticulin (CRT) and high mobility group protein B1 (HMGB1), were up-regulated compared to PBS group, and the down-regulated of HIF-α-A2AR revealed the manifestation of CS@M NPs in immune activation (Fig. S18D in Supporting information). The findings showed a variety of potential mechanisms by which CS@M NPs could inhibit the growth of tumors, pointing to a critical role for the enhanced PDT strategy in reversing the hypoxic environment in tumors.

Fig. 4A demonstrated that in the presence of PDT, both free Ce6 and nanoparticles significantly increased the ICD effects on cells. Further, the CD39-CD73-A2AR pathway of PDT was verified, and the results showed that CS@M NPs significantly inhibited the expression of CD39, CD73, and A2AR, thus blocking the inhibitory effect of this pathway on the immune system (Fig. 4B). Adenosine concentration significantly dropping also supported the impact of CS@M NPs on the A2AR pathway (Fig. 4C). The alterations of immune-related cytokines in mice's serum following treatment with various formulations were investigated to confirm the immune activating effect of nanoparticles. As seen in Fig. 4D, the nanoparticles group experienced an increase in IL-12, IL-2, tumor necrosis factor-alpha (TNF-α), and interferon-gamma (IFN-γ), with CS@M NPs showing the best induction. FCM was used to verify the close relationship between DC cell maturation and T cell activation with A2AR and the above cytokines: CS@M NPs effectively induced DC cell maturation and tumor immune infiltration of $CD8^+$ T cells (Fig. 4E). A more precise and effective tumor immunotherapy with $CD8^+$ T cells was made possible thanks to the DC cell antigen presentation due to the ICD effect. The PDT and ICD of hypoxic tumor cells are fully utilized by CM@NPs to improve the effectiveness of tumor suppression and serve as a crucial point of reference for the management of TNBC.

In summary, a 4T1 cell membrane camouflaged nanoplatform was created constructed based on the co-assembly of Ce6-S-S-LA and SQ. The biomimetic nanodrug exhibited a greatly increased cellular uptake of homogeneous cells *in vitro* as well as increased the specific self-recognition of tumors *in vivo*. The synthesis of Ce6-S-S-LA allowed the self-assembly characteristics of nanoparticles and the disulfide bonding ensured the GSH-responsive release of SQ and Ce6 in tumor environment. SQ not only provided sufficient oxygen, but also reversed tumor hypoxia and achieved enhanced PDT. RNA sequencing results demonstrated the potential role of the CS@M NPs in immune system activation. By inhibiting the expression of HIF-α-CD39-CD72-A2AR pathway, CS@M NPs sig-

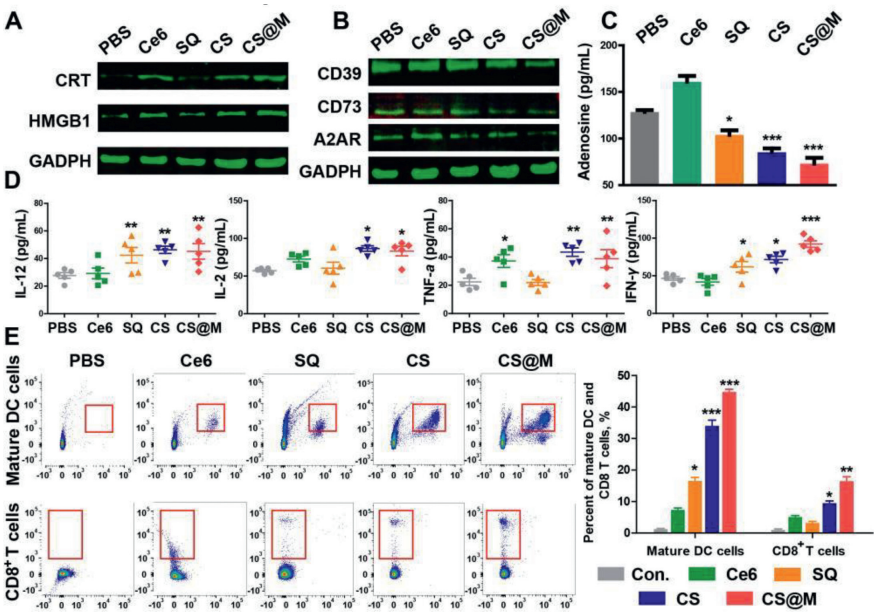

Fig. 4. Study of the *in vivo* immune activation effect of CS@M NPs. (A, B) The protein expression of CRT, HMGB1, CD39, CD73 and A2AR in co-cultured PBMC and 4T1 cells after treated with different drugs. (C) Intracellular adenosine concentration determined by enzyme-linked immunosorbent assay (ELISA). (D) Quantitative analysis of the expression of the cytokines (IL-12, IL-2, TNF-α, IFN-γ) in the serum of various groups of mice. (E) DC cells maturation in blood and $CD8^+$ T cells in tumor sites examined by FCM. Data were expressed as the mean ± SD ($n = 3$). $^*P < 0.05$, $^{**}P < 0.01$, $^{***}P < 0.001$.

nificant promoted the DC cells maturation and $CD8^+$ T cells proliferation. In addition, ICD effect was confirmed by the secretion of ICR and HMGB1, PDT provided specific tumor antigens for DC to enhance the cytotoxic T lymphocyte (CTL) immune infiltration to tumors. Synergistic photodynamic immunotherapy with CS@M NPs showed superiority in eliminating hypoxic tumors and provides new options for the clinical treatment of TNBC.

Declaration of competing interest

The authors declare that they have no known competing financial interests or personal relationships that could have appeared to influence the work reported in this paper.

Acknowledgments

This work was supported by the Guangdong Nature Resource Center (No. (2020)037) and Natural Science Foundation of Guangdong Province (Nos. 22019A1515011498 and 2019A1515011619); Basic and Applied Basic Research Foundation of Guangdong Province (No. 2020B15151 20063); National Natural Science Foundation of China (No. 81803877). The research was also supported by the China Postdoctoral Science Foundation (No. 2022M721535).

Supplementary materials

Supplementary material associated with this article can be found, in the online version, at doi:10.1016/j.cclet.2023.108518.

References

[1] M. Nedeljkovic, A. Damjanovic, Cells 8 (2019) 957.
[2] R.L. Siegel, K.D. Miller, A. Jemal, CA Cancer J. Clin. 69 (2019) 7–34.
[3] J.C. Li, X.Z. Liu, L. Chen, et al., Toxicol. Appl. Pharmacol. 462 (2023) 116415.
[4] Z.Z. Yu, P. Zhou, W. Pan, et al., Nat. Commun. 9 (2018) 5044.
[5] K.X. Teng, L.Y. Niu, Q.Z. Yang, J. Am. Chem. Soc. 145 (2023) 4081–4087.
[6] X.L. Guo, N.D. Yang, W.H. Ji, et al., Adv. Mater. 33 (2021) e2007778.
[7] K.X. Teng, L.Y. Niu, N. Xie, et al., Nat. Commun. 13 (2022) 6179.
[8] K.X. Teng, W.K. Chen, L.Y. Niu, et al., Angew. Chem. Int. Ed. 60 (2021) 19912–19920.
[9] S.Y. Zhou, X.L. Hu, R. Xia, et al., Angew. Chem. Int. Ed. 59 (2020) 23198–23205.
[10] J.Q. Huang, L.P. Zhao, X. Zhou, et al., Small 18 (2022) e2107467.
[11] M. Hu, Y.F. Li, Y.T. Lu, et al., Peer J. 9 (2021) e11306.
[12] Z.K. Zhang, J.C. Kuo, C. Zhang, et al., Pharmaceutics 13 (2021) 2060.
[13] Y. Takemoto, S. Kadota, I. Minami, et al., Angew. Chem. Int. Ed. 60 (2021) 21824–21831.
[14] J. Caron, A. Maksimenko, S. Wack, et al., Adv. Healthc. Mater. 2 (2013) 172–185.
[15] Y.Y. Jin, B.B. Zhao, W.J. Guo, et al., J. Control. Release 348 (2022) 911–923.
[16] Sun C.L, J.C. Wang, H.L. Gao, et al., Acta Pharm. Sin. B 9 (2019) 1145–1162.
[17] Z. Wang, F.H. Meng, Z.Y. Zhong, Adv. Drug. Deliv. Rev. 178 (2021) 113969.
[18] H.L. Sun, Y.F. Zhang, Z.Y. Zhong, Adv. Drug. Deliv. Rev. 132 (2018) 16–32.
[19] X.L. Gu, Y.H. Wei, Q.Y. Fan, et al., J. Control. Release 301 (2019) 110–118.
[20] S.Y. Wang, K.Y. Yu, Z.Z. Yu, et al., J. Control. Release 329 (2021) 676–695.
[21] P.P. Xu, X.Y. Wang, T.W. Li, et al., Chin. Chem. Lett. 34 (2023) 108184.
[22] Y.X. Lin, Y. Wang, H.W. An, et al., Nano Lett. 19 (2019) 2968–2978.
[23] X.Y. Xu, Z.S. Zeng, X. Ding, et al., Biomaterials 277 (2021) 121128.
[24] B.C. Zhang, J.L. Jiang, P.Y. Wu, et al., Acta Pharm. Sin. B 11 (2021) 246–257.
[25] Z.Z. Zhang, Y.X. Yue, L.N. Xu, et al., Adv. Mater. 33 (2021) e2007719.
[26] T. Zhong, X. Yao, S. Zhang, et al., Sci. Rep. 6 (2016) 36614.
[27] G.T. Li, B.J. Sun, Y.Q. Li, et al., Small 17 (2021) e2101460.
[28] J.G. Wang, J.Y. Zhuo, Y.Y. Tao, et al., Int. J. Nanomedicine 15 (2020) 6839–6854.
[29] Z.Y. Mai, J. Zhong, J.S. Zhang, et al., ACS Nano 17 (2023) 1583–1596.
[30] L.M. Wu, F. Zhang, X.N. Chen, et al., ACS Appl. Mater. Interfaces 12 (2020) 3327–3340.
[31] B.J. Sun, C. Luo, H. Yu, et al., Nano Lett. 18 (2018) 3643–3650.
[32] N. Wang, Z.Q. Deng, Q. Zhu, et al., Chem. Sci. 12 (2021) 14353–14362.
[33] Y. Xiao, T. Zhang, X.B. Ma, et al., Adv. Sci. 8 (2021) e2101840.
[34] F. Zhuang, Q. Ma, C.H. Dong, et al., ACS Nano 16 (2022) 5439–5453.
[35] Z. Li, Q. Xu, X. Lin, et al., Chin. Chem. Lett. 33 (2022) 1875–1879.
[36] H.J. Wang, Y. Liu, R.Q. He, et al., Biomater. Sci. 8 (2020) 552–568.
[37] Z. Chen, P.F. Zhao, Z.Y. Luo, et al., ACS Nano 10 (2016) 10049–10057.
[38] X.C. Pei, X.H. Pan, X.Y. Xu, et al., Biomater. Sci. 9 (2021) 1325–1333.